Article ID: 1000-7032(2023)09-1681-12

Construction of Quantum Dot-modified *Ln*-ZIF Hybrid Materials and Fluorescence Detection of Tannic Acid

FANG Zhou, JIA Dongsheng, LI Tianming, LI Ying*, ZHANG Dongliang*

(*School of Materials & Chemistry, University of Shanghai for Science and Technology, Shanghai* 200093, *China*)

* *Corresponding Authors, E-mail: liying@usst. edu. cn; zdl*20003@*usst. edu. cn*

Abstract: Lanthanide Eu^{3+}-doped metal-organic backbone material Eu/ZIF-67 was prepared by a one-step hydrothermal method with a novel pleated sphere structure. A dual-emission fluorescent hybrid material Eu/ZIF-67@ZnO QDs with a zeolite imidazolium ester backbone was obtained by loading ZnO quantum dots onto the surface of Eu/ZIF-67 *via* coordination bonding. The structure, morphology and fluorescence sensing properties of the material were characterized in detail. Furthermore, the fluorescent material was found to display the dual fluorescence emission of ZnO quantum dots and lanthanide red europium ions. The fluorescence sensing performance of Eu/ZIF-67@ZnO QDs to tannic acid was further investigated, and the results indicated that tannic acid can effectively burst the characteristic fluorescence emission of Eu/ZIF-67@ZnO QDs at ZnO QDs with a detection limit of 0. 029 9 μmol/L. Meanwhile, Eu/ZIF-67@ZnO QDs have the fluorescence response to tannic acid with anti-interference ability, which can be used as a cost-effective fluorescence sensor to specifically identify tannic acid.

Key words: metal organic skeleton; quantum dots; dual-emission probes; tannic acid; fluorescent detection

CLC number: TB333 **Document code**: A **DOI**: 10. 37188/CJL. 20230048

量子点修饰 *Ln*-ZIF 杂化材料的构筑及其对单宁酸的荧光检测

方 舟, 贾东升, 李天铭, 李 颖*, 张栋梁*

(上海理工大学 材料与化学学院, 上海 200093)

摘要: 采用一步水热法制备了一种具有新型褶皱球结构的镧系金属 Eu^{3+} 掺杂的金属有机骨架材料 Eu/ZIF-67,并进一步通过配位键合的方式将 ZnO 量子点负载到 Eu/ZIF-67 的表面,形成了一种类沸石咪唑酯骨架的双发射荧光杂化材料 Eu/ZIF-67@ZnO QDs。通过对材料的结构、形貌以及荧光传感性能表征分析,发现该荧光材料具有 ZnO 量子点和镧系红光铕离子的双重荧光发射。此外,进一步探究了 Eu/ZIF-67@ZnO QDs 对单宁酸的荧光传感性能。结果表明,单宁酸能够有效猝灭 Eu/ZIF-67@ZnO QDs 在 ZnO QDs 处的特征荧光发射,检出限为 0.029 9 μmol/L。同时,Eu/ZIF-67@ZnO QDs 对单宁酸的荧光响应具有抗干扰能力,可作为一种经济高效的荧光传感器来特异性识别单宁酸。

关 键 词: 金属有机骨架; 量子点; 双发射探针; 单宁酸; 荧光检测

收稿日期: 2023-03-01; **修订日期**: 2023-03-14

基金项目: 国家自然科学基金(21101107,51173107); 同济大学污染控制与资源化国家重点实验室基金项目(PCRRF19017)
Supported by National Natural Science Foundation of China(21101107,51173107); State Key Laboratory of Pollution Control and Resource Reuse Foundation(PCRRF19017)

1 Introduction

Tannins, or ellagic acid, is a multiphase phenolic compound widely distributed in nature and can be mainly classified into three categories: hydrolyzed tannins (HT), condensed tannins (CT) and fucoidan polyphenols (PT)[1-3]. The polyphenolic hydroxyl structure of tannins gives them a unique set of chemical properties and physiological activities, making them valuable in food, pharmaceutical and industrial production applications. The polyphenolic structure of tannins allows them to combine with proteins and alkaloids, as well as to complex and electrostatically interact with many metal ions, and to possess antioxidant and anti-inflammatory properties[4-9]. Therefore, tannins can be used as food antioxidants, detoxifying agents, sunscreen skin brighteners, topical coagulants, clarifying agents for beer and wine, coagulants for rubber, *etc*. [10]. In beer brewing, tannic acid can form precipitates with proteins in the wort, clarifying and making the beer transparent. However, excessive intake of tannic acid also has certain adverse effects on the human body, therefore, as a widely used food additive, the concentration level of tannic acid not only affects the flavor of food, but also plays a standard role in evaluating the quality of food[11-12]. Currently, the detection of tannins mainly includes spectrophotometric[13], electrochemical[14-15], chromatographic[16] and colorimetric[17] methods. Although there are various detection methods, most of them exist poor selection specificity, complicated pre-processing or operation, expensive machine cost, and other problems, hence, it is of practical significance to explore a method for the accurate, rapid, and effective detection of tannins.

Quantum dots are quasi-zero-dimensional nanomaterials with a semiconducting nanostructure in which electrons are bound in all three directions. With the ability to modify the emission spectrum by modulating the size and chemical composition, quantum dots also have excellent photostability, large Stokes shifts, low cytotoxicity, and high stability[18-20]. Therefore, they have a wide range of applications in recent decades in the fields of biofluorescent labeling, luminescent devices, and fluorescence detection[21-25]. Among them, ZnO quantum dots are a novel semiconductor nanomaterial with a forbidden band width of 3.37 eV[26], which have great potential for applications in fluorescence detection and matter sensing due to their good biocompatibility and excellent optoelectronic properties[27-29]. Metal organic framework materials (MOFs) are a class of porous crystalline materials with a regular network structure formed by metal ions or clusters as the central binding ligands. MOFs have in-depth investigations and applications in sensing and storage separation of gases, catalysis, and drug mitigation due to their high specific surface area, low crystal density, tunable pore size, and easily modified functional structures[30-33]. Due to metal-organic framework materials have the features of designable pore surface functional sites and adjustable ligands, novel framework structures can be continuously designed to expand the application fields of lanthanide MOFs by introducing different central metal ions, loading, or embedding nanomaterials and designing novel ligands.

Herein, we designed a simple & green strategy to construct a dual-emitting metal organic skeleton material. The yellow-emitting ZnO quantum dots were prepared by a chemical solution method and capped with amino groups to obtain amino-functionalized ZnO quantum dots; then a novel zeolite-like imidazolium ester backbone was constructed by doping with Co and lanthanide metal Eu to obtain a novel pleated sphere structured metal-organic framework. By loading ZnO quantum dots, a fluorescent hybrid material with double emission is finally obtained, which can realize the sensing detection of tannic acid and provide a simple and feasible method for the rapid and effective detection of tannic acid concentration.

2 Experiment

2.1 Preparation of Eu/ZIF-67@ZnO QDs

2.1.1 Experimental Reagents

$Eu(NO_3)_3 \cdot 6H_2O$, $Zn(OAc)_2 \cdot 2H_2O$, L-arginine, L-alanine, glycine, L-aspartic acid, gallic acid, ellagic acid, (3-aminopropyl) tri-ethoxysilane (APTES),

2-Methylimidazole, KBr and tannic acid (TA) were purchased from Adamas-beta Co., Ltd. (Shanghai, China). Methyl alcohol, L-ascorbic acid (AA), $MgCl_2$, NaCl, $CuCl_2$, $FeCl_3 \cdot 6H_2O$, $FeCl_2 \cdot 4H_2O$, $ZnCl_2$, KOH and $CoCl_2 \cdot 6H_2O$ were purchased from Sinopharm Chemical Reagent Co., Ltd. (Shanghai, China). Toluene, anhydrous ethanol, glucose, and sucrose were purchased from Shanghai Aladdin Biochemical Technology Co., Ltd. (Shanghai, China).

2.1.2　Preparation Process

(1) Preparation of amino-functionalized ZnO QDs

The 2.79 mmol of $Zn(OAc)_2 \cdot 2H_2O$ was added to 15 mL of anhydrous ethanol in a water bath at 78 ℃ and refluxed under vigorous stirring until completely dissolved. The 6 mol of KOH was dissolved in anhydrous ethanol and refrigerated to 4 ℃, then slowly add dropwise to the ethanol solution of $Zn(OAc)_2 \cdot 2H_2O$. After stirring for 60 min at room temperature, 0.5 mmol of APTES was added to anhydrous ethanol/water (anhydrous ethanol: water = 10∶1), mixed well and added to the above reaction system, and continued to stir at room temperature for 6 h. After the reaction was completed, the precipitate was washed several times by centrifugation with toluene and anhydrous ethanol and dried, and the white translucent solid was obtained as ZnO QDs.

(2) Synthesis of Eu-doped ZIF-67

The mixture of 0.95 mmol of $CoCl_2 \cdot 6H_2O$ and 0.05 mmol of $Eu(NO_3)_3 \cdot 6H_2O$ was dissolved in 10 mL of deionized water as solution A. The 20 mmol of 2-methylimidazole was dissolved in 10 mL of deionized water as solution B. After adding B to A and sonicating for 5 min, the mixed system was placed in a 50 mL reactor at 120 ℃ for 1 h. When reaction was finished, the mixture was washed several times by centrifugation using methyl alcohol and water, respectively, and dried to obtain the purple solid as Eu/ZIF-67.

(3) Construction of Eu/ZIF-67@ZnO QDs

The 20 mg of Eu/ZIF-67 was ultrasonically dispersed in 10 mL of deionized water, and 30 mg of ZnO QDs was dispersed in 10 mL of deionized water. The ZnO QDs solution was added dropwise to the aqueous solution of Eu/ZIF-67, stirred for 12 h at room temperature, and then centrifuged to obtain Eu/ZIF-67@ZnO QDs (Fig. 1).

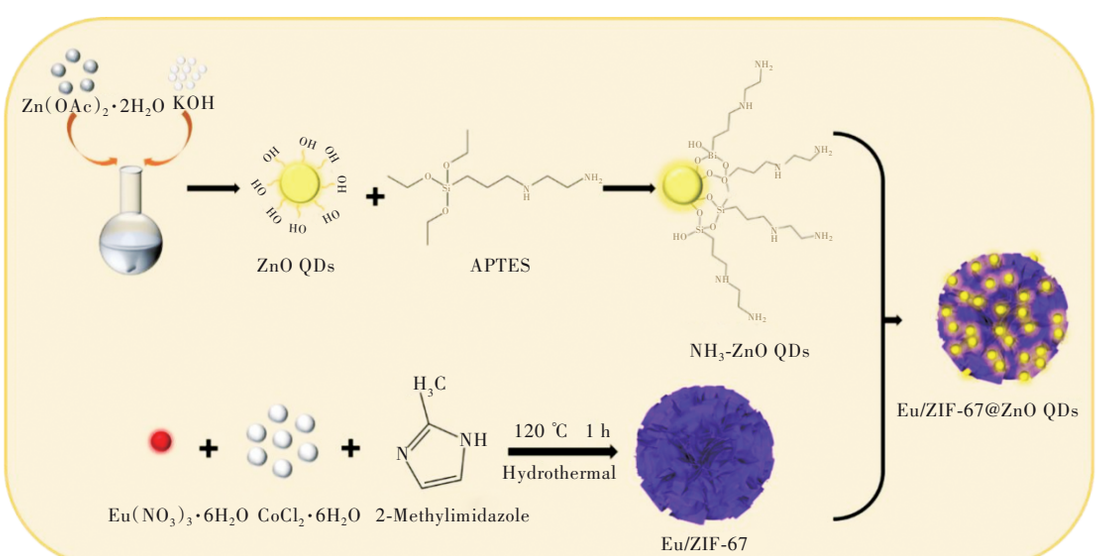

Fig.1　Experimental process and schematic diagram of Eu/ZIF-67@ZnO QDs

(4) Sensing detection of tannic acid (TA)

Eu/ZIF-67@ZnO QDs were configured into a homogeneous solution, to which a series of TA solutions with different concentrations were added dropwise, and the fluorescence intensity changes were measured using a fluorescence spectrometer. The concentration range of the added TA solution was 0.01−1 μmol/L. The fluorescence emission spectrum was measured at the excitation wavelength of 356 nm, where the emission wavelength was 505 nm

for ZnO QDs and 615 nm for Eu/ZIF-67@ZnO QDs. The slit of the instrument was 5 nm in all fluorescence tests.

2.2 Performance and Characterization of Samples

The chemical structure of the samples was characterized by potassium bromide compression and scanned on a Fourier transform infrared spectroscopy (FT-IR) SPECTRUM 100 FT-IR spectrophotometer (Perkin Elmer, USA) at 4 000−400 cm^{-1}. Scanning electron microscopy (SEM) was performed on a ZEISS Sigma 300 (Germany) with acceleration voltage E_{HT} = 3.0 kV. Powder X-ray diffraction (XRD) was determined on a D8 ADVANCE X-ray diffractometer. The UV-Vis absorption spectra of the samples were obtained by analysis on a UV-Vis spectrometer(Lambda FEG450). The samples were analyzed for elemental content and functional group types using X-ray photoelectron spectroscopy (XPS) with a Thermo Scientific K-Alpha+, monochromatic AI Kα X-ray source(1 486.6 eV) at 12 kV and 72 W, respectively, instrument model and parameters. Fluorescence spectroscopy tests were obtained on a Shimadzu S220 V fluorescence spectrophotometer and an Edinburgh FLS920 fluorescence spectrometer with excitation sources of 450 W xenon lamp, μF 920H pulsed light source and EPL-375 nanosecond light source.

3 Results and Discussion

3.1 Structural Characterization of ZnO QDs, Eu/ZIF-67 and Eu/ZIF-67@ZnO QDs

The surface morphology before and after the Eu/ZIF-67 composite ZnO QDs was characterized by scanning electron microscopy (E_{HT} =3.00 kV, M_{ag}= 50.00 KX, Signal A=SE2, W_D=7.9 mm). As the Fig. 2(a) describes, the surface of the Eu-doped ZIF-67 is richly folded and has an overall spherical shape with a diameter of about 1.2 μm. The introduction of ZnO QDs resulted in fewer folds on the surface of the irregular spheres and many particles loaded on the surface, leading to a slight increase in the particle size of the spheres. The above results suggest that the ZnO QDs are probably loaded on the surface of the Eu/ZIF-67 skeleton by chemical bonding, and their introduction would not cause the collapse of the skeleton structure.

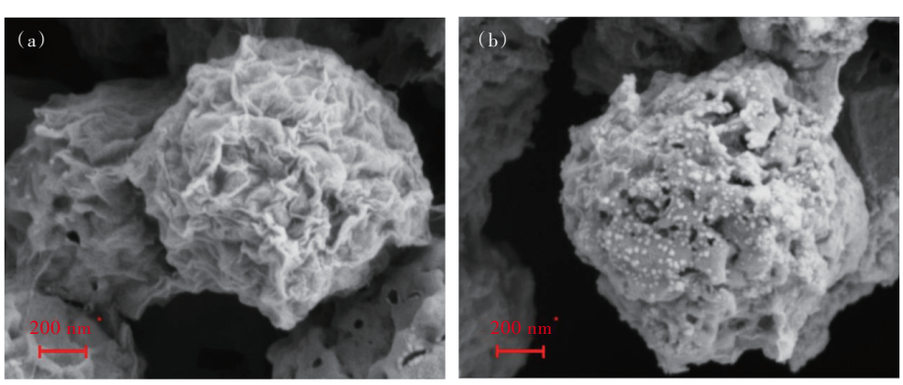

Fig.2 The SEM images of Eu/ZIF-67(a) and Eu/ZIF-67@ZnO QDs(b)

The chemical structures of ZnO QDs (a), ZIF-67 (b), Eu/ZIF-67 (c) and Eu/ZIF-67@ZnO QDs (d) were characterized by FT-IR. As Fig. 3 suggests, where the broadband at 3 469 cm^{-1} is attributed to the O—H stretching vibration and the absorption peaks at 2 925 cm^{-1} and 3 134 cm^{-1} are attributed to the C—H stretching vibration. Line a corresponds to ZnO QDs, where the absorption peak at 1 595 cm^{-1} is attributed to N—H and the absorption band near 1 000 cm^{-1} is attributed to the Si—O band from APTES. These characteristic peaks indicate that APTES was successfully encapsulated on the surface of ZnO QDs and ZnO QDs were successfully amino-functionalized[34-36]. Among the lines b, c and d, the peak clusters in the range of 680−1 500 cm^{-1} are attributed to the stretching and bending vibrations of the imidazole ring, the absorption peak at 1 598 cm^{-1} is attributed to the stretching

vibrations of C—N, and the broad absorption band at 1 044 cm^{-1} in d is attributed to Si—O in ZnO QDs[37-38]. The above results indicate the successful preparation of ZnO QDs and zeolite-like imidazole ester frameworks, and the introduction of ZnO QDs didn't destroy the skeleton structure of Eu/ZIF-67.

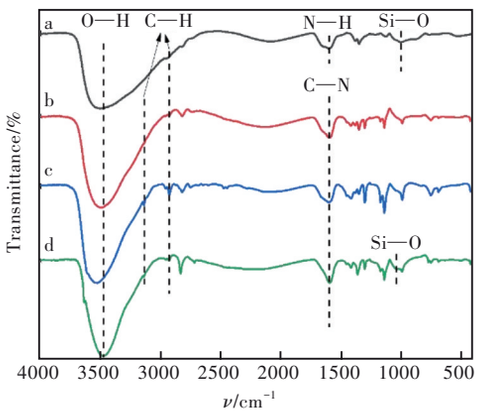

Fig.3　FT-IR spectrum of ZnO QDs(a), ZIF-67(b), Eu/ZIF-67(c) and Eu/ZIF-67@ZnO QDs(d).

The crystal structures of ZnO QDs, ZIF-67, Eu/ZIF-67 and Eu/ZIF-67@ZnO QDs were characterized by X-ray powder diffraction. As described in Fig. 4, Eu/ZIF-67 and Eu/ZIF-67@ZnO QDs exhibit the same crystal structure at 2θ=7.39°(011), 10.38°(002), 12.75°(112), 14.70°(022), 16.47°(013), 18.06°(222), 22.14°(114), 24.50°(233), 26.70°(134), which corresponds exactly to the ZIF-67 in the literature[37-38]. They demonstrate that the introduction of ZnO QDs did not cause the collapse of the crystal structure of Eu/ZIF-67. The ZnO QDs exhibit broad peaks at 31.78°(001), 34.47°(002), 36.15°(101), demonstrating the successful preparation of ZnO QDs. Furthermore, the characteristic peaks at 36.46° and 34.54° for Eu/ZIF-67@ZnO QDs are attributed to the combination of ZnO QDs with Eu/ZIF-67, further demonstrating the successful preparation of europium ion-doped zeolite-like imidazolium-based frameworks and Eu/ZIF-67 with ZnO QDs.

The elemental composition of the prepared Eu/ZIF-67@ZnO QDs was analyzed by XPS. This material shows the characteristic peaks of C, O, N, Co, and Eu at 284.73, 530.95, 398.82, 781.03,

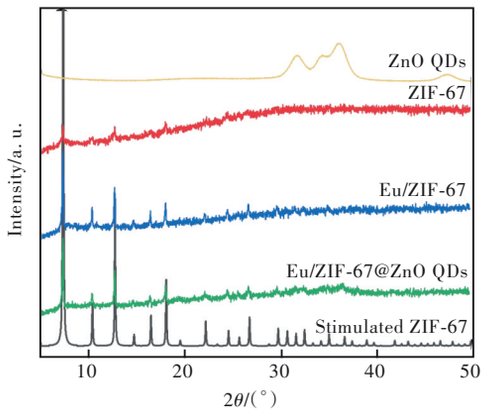

Fig.4　XRD spectrum of ZnO QDs, ZIF-67, Eu/ZIF-67, Eu/ZIF-67@ZnO QDs and stimulated ZIF-67.

1 134.71 eV, respectively. The contents of these five elements are 46.93%(C), 21.94%(O), 13.81%(N), 4.33%(Co), and 0.79%(Eu). Fig. 5(b)-(f) represents the fine spectrum of C 1s, O 1s, N 1s, Co 2p, and Eu 3d, respectively. For the C 1s spectrum, three peaks appear at 284.3, 284.9, 285.6 eV, which correspond to the characteristic peaks of C—C/C=C, N—C=N and C—O, respectively; for the O 1s spectrum, there are three peaks at 530.1, 531.1, 531.9 eV, indicating the presence of *M*—O(*M* for Zn, Co, Eu), Si—O and materials in the sample that indicate the possible adsorption of presence of water, and also demonstrates the successful introduction of ZnO QDs[36,39]. For the N 1s spectrum, the peaks at 398.4, 398.9, 399.4, 400.4 eV can be attributed to C=N—C, Co—N, C—NH—C and N—O, respectively. the Co 2p spectrum is composed of two energy levels concentrated at 780.9 eV and 796.9 eV, respectively, attributed to Co $2p_{3/2}$ and Co $2p_{1/2}$. The peaks at 780.7, 782.3, 786.5 eV can be attributed to Co^{2+}, Co^{3+} and a satellite peak, respectively[37-38]. For the Eu 3d spectrum, 1 134.7 eV and 1 164.9 eV correspond to the Eu $3d_{5/2}$ and Eu $3d_{3/2}$ energy levels, respectively[40]. For the Zn 2p spectrum, 1 021.6 eV and 1 044.6 eV correspond to two energy levels, Zn $2p_{3/2}$ and Zn $2p_{2/1}$, respectively. The above results are consistent with the FT-IR spectral results, further indicating the successful synthesis of Eu/ZIF-67@ZnO QDs.

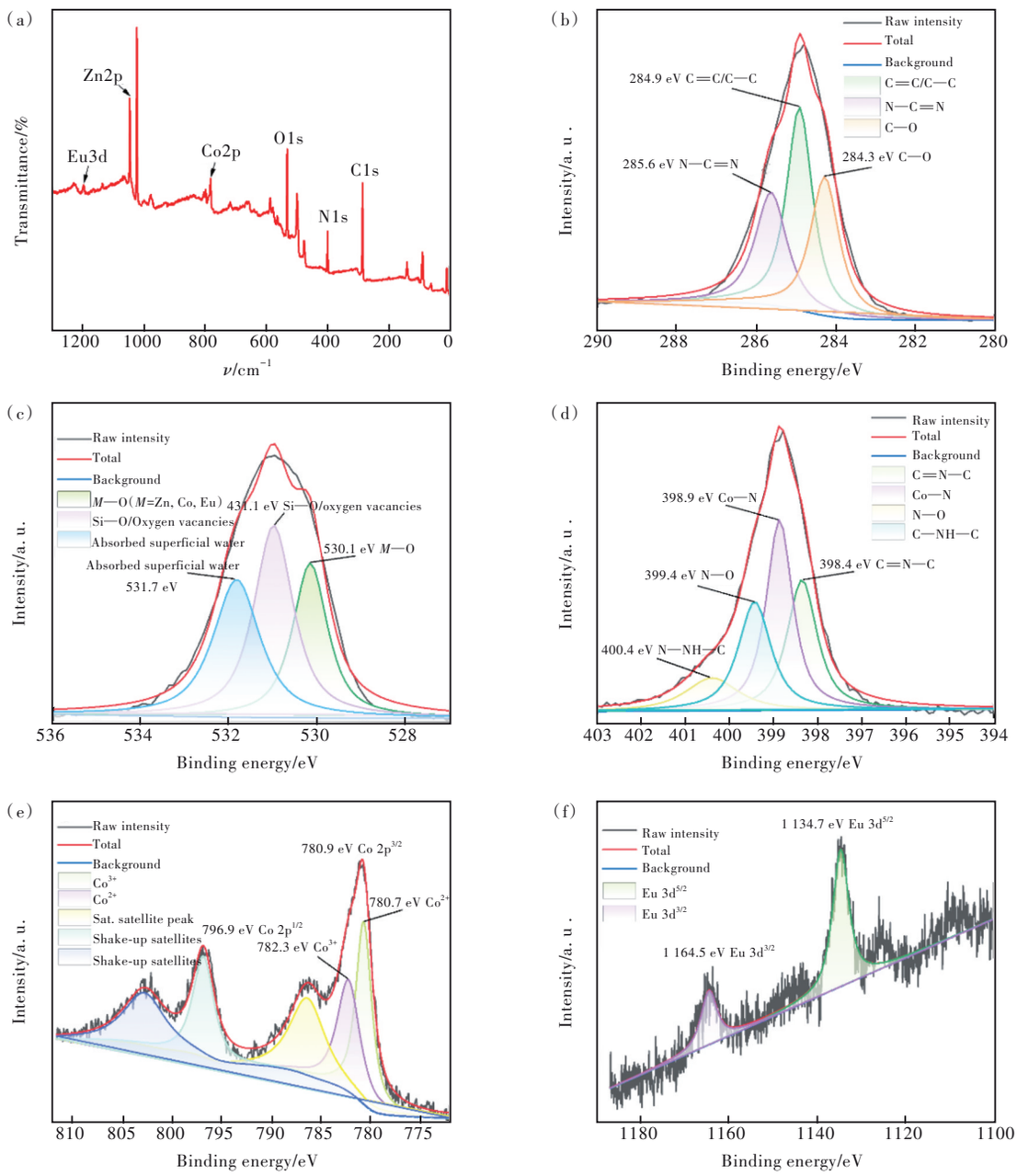

Fig.5 (a)XPS spectrum of Eu/ZIF-67@ZnO QDs. (b)C 1s spectrum of Eu/ZIF-67@ZnO QDs. (c)O 1s spectrum of Eu/ZIF-67@ZnO QDs. (d)N 1s spectrum of Eu/ZIF-67@ZnO QDs. (e)Co 2p spectrum of Eu/ZIF-67@ZnO QDs. (f)Eu 3d spectrum of Eu/ZIF-67@ZnO QDs.

Tab.1 The XPS survey of Eu/ZIF-67@ZnO QDs of each element

Name	Start BE	Peak BE	End BE	Atomic/%	PP At. /%
Eu 3d	1 186. 78	1 134. 71	1 100. 18	0. 79	0. 2
C 1s	297. 98	284. 73	279. 18	46. 93	54. 03
Co 2p	811. 98	781. 03	771. 18	4. 33	1. 41
Zn 2p	1 051. 98	1 021. 56	1 015. 18	12. 2	7. 8
N 1s	409. 98	398. 82	392. 18	13. 82	16. 97
O 1s	544. 98	530. 95	525. 18	21. 94	19. 59

3.2　Fluorescent Properties of Eu/ZIF-67@ZnO QDs

The excitation and generation spectra of the prepared ZnO QDs and Eu/ZIF-67@ZnO QDs were measured using a fluorescence spectrometer at room temperature. As shown in Fig. 6(a), the optimal emission spectrum, and the optimal excitation spectrum of the ZnO QDs were determined at the excitation wavelength of 356 nm and the emission wavelength of 572 nm, respectively. Fig. 6(b) indicates that the optimal emission spectra and the optimal excitation spectra of Eu/ZIF-67@ZnO QDs were determined at 356 nm excitation wavelength and 615 nm emission wavelength, respectively, where the emission peak at 554 nm was attributed to the yellow emission of ZnO QDs and the emission peak at 615 nm was attributed to the characteristic jump of Eu at $^5D_0$-$^7F_2$. The two emission peaks surface the successful doping of Eu and the successful introduction of ZnO QDs.

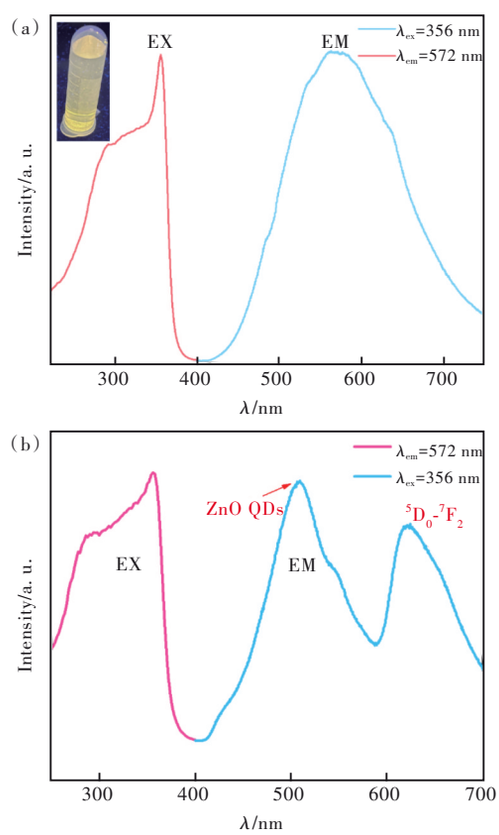

Fig.6　(a) The optimal excitation and emission spectrum of ZnO QDs (inset is a photograph of aqueous ZnO QDs under a 365 nm UV lamp). (b) The optimal excitation and emission spectrum of Eu/ZIF-67@ZnO QDs.

To investigate the sensitivity of Eu/ZIF-67@ZnO QDs for the detection of TA, the fluorescence response of this fluorescent probe to different concentrations of TA was carried out. Firstly, time and temperature conditions optimization experiments were carried out for the detection of TA. Fig. 7(c)-(d) illustrate that, when TA was added, the fluorescence response value of Eu/ZIF-67@ZnO QDs completed the response within 1 min with little subsequent change as the time increased. Then the response of Eu/ZIF-67@ZnO QDs to TA was investigated at different incubation temperatures. The fluorescence response decreases continuously as the temperature increases. Considering the environmental temperature of 20-28 ℃ for TA in beer brewing, 25 ℃ was chosen as the real-time detection temperature. Fig. 7(a) reveals that the fluorescence intensity of Eu/ZIF-67@ZnO QDs at both quantum dots and rare earth ions gradually decreases with the increase of TA concentration, we selected the fluorescence intensity change at ZnO QDs as the response signal. As shown in Fig. 7(b), it can be analyzed that the probe has a good fluorescence response to TA in the concentration range of 0-0.2 μmol/L, and its weakening trend is well in line with the first order exponential decay, and the fluorescence response value (F/F_0) shows a good linear relationship with the concentration of TA. A linear fit was performed to obtain a linear regression equation of $y = -0.8471x + 0.9699$ ($R^2 = 0.996$). The fit was calculated using the Stern-Volmer equation as follows.

$$\frac{F}{F_0} = 1 + K_{SV}C, \tag{1}$$

where C is the concentration of tannic acid (TA), K_{SV} is the Stern-Volmer constant, F is the fluorescence intensity at ZnO QDs after the addition of TA, and F_0 is the fluorescence intensity of blank Eu/ZIF-67@ZnO QDs at ZnO QDs. The detection limit (LOD) D of the probe for TA can be calculated from the 3σ equation as 0.029 9 μmol/L:

$$D = 3\sigma/S, \tag{2}$$

σ is the standard deviation obtained from 20 consecutive scans of the probe blank solution, and S is the

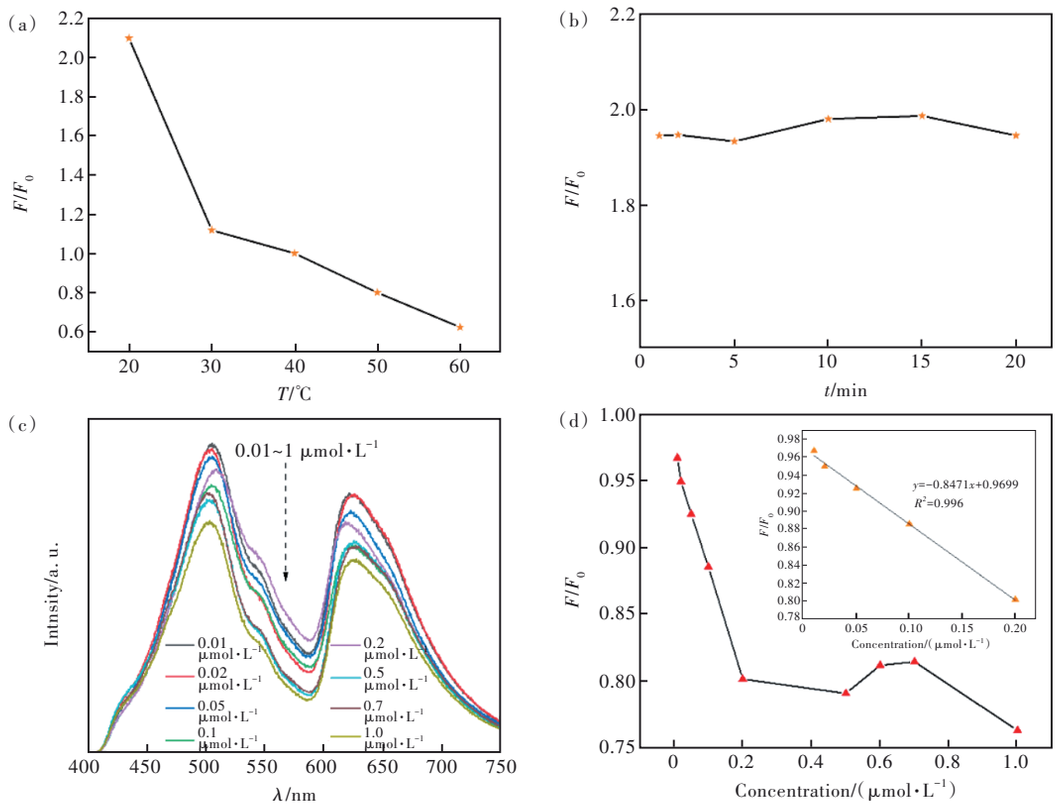

Fig.7 The fluorescence response values(F/F_0) of Eu/ZIF-67@ZnO QDs to TA with respect to temperature(a) and reaction times (b). The fluorescence emission spectrum of Eu/ZIF-67@ZnO QDs after the addition of different concentrations of TA(λ_{ex}= 356 nm)(c) and fluorescence response values(F/F_0) *versus* TA concentration(inset is a linear plot)(d).

slope of the linear regression equation.

We compared the Eu/ZIF-67@ZnO constructed in this work with the recent related work. As shown in Tab. 2, it is observed that the Eu/ZIF-67@ZnO fluorescent probe prepared in this work possesses better sensitivity and lower detection limit for the detection of TA. From the above results, it is concluded that the Eu/ZIF-67@ZnO QDs probe has good fluorescence sensing properties for TA and can be used as an excellent sensor to measure the concentration level of TA.

Tab. 2 The comparison table of Eu/ZIF-67@ZnO for detecting TA with other works

Materials	Method	LOD	Refs.
FNCDs-H_2O_2-$K_3Fe(CN)_6$	Chemiluminescence	39.3 nmol·L^{-1}	[41]
BPEI-CDs	Fluorescence spectroscopies	36.8 nmol·L^{-1}	[42]
Fe_2O_3 NPs embedded porous films	Colorimetric detection	370 nmol·L^{-1}	[43]
PEG/CPE	Electrochemical methods	72.6 nmol·L^{-1}	[44]
NH_2-GQDs	Fluorescence determination	43.3 nmol·L^{-1}	[45]
CdS/TiO_2/FTO	Electrochemical methods	10 μmol·L^{-1}	[46]
Eu/ZIF-67@ZnO QDs	Fluorescence determination	29.9 nmol·L^{-1}	This work

To further investigate the specificity and selectivity of Eu/ZIF-67@ZnO QDs probes for the detection of TA, anti-interference tests were performed for common substances, including Mg^{2+}, Na^+, Cu^{2+}, Ca^{2+}, Zn^{2+}, Fe^{2+}, Fe^{3+}, Cl^-; the common amino acids L-arginine, L-ascorbic acid (AA), L-alanine, glycine, L-aspartic acid, gallic acid, and ellagic acid; sugars such as glucose, sucrose. The concentration of TA was 0.01 μmol/L and the concentration of all other interfering substances was 1 μmol/L. We examined the fluorescence response changes of the Eu/ZIF-67@ZnO QDs probes for these substances. Compared with other anti-interference substances, tannic acid can effectively burst the fluorescence of Eu/ZIF-67@ZnO QDs(Fig. 8). These results demonstrate that Eu/ZIF-67@ZnO QDs can be used as a fluorescent

sensor with good sensitivity and specificity for the selective detection of TA.

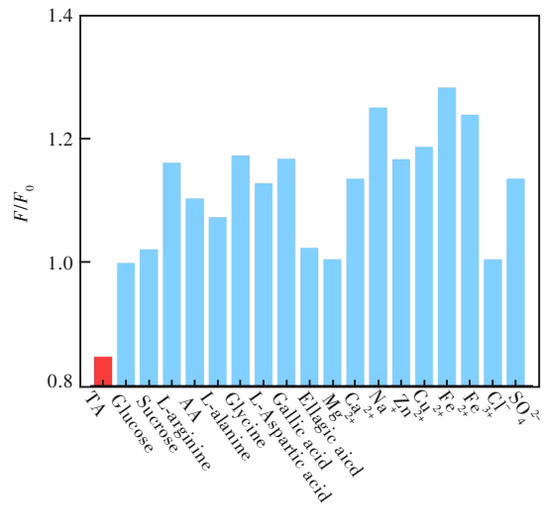

Fig.8　The fluorescence emission spectrum of Eu/ZIF-67@ZnO QDs after dropwise addition of different anti-interference substances at 356 nm (F is the fluorescence intensity at ZnO QDs after the addition of different anti-interference substances, and F_0 is the fluorescence intensity of blank Eu/ZIF-67@ZnO QDs at ZnO QDs).

3.3　Possible Mechanism of Fluorescence Quenching of Eu/ZIF-67@ZnO QDs

The UV absorption spectra of Eu/ZIF-67@ZnO QDs and the detection substance tannic acid (TA) were scanned by UV-Vis spectrophotometer. From the absorption spectrum of TA, it can be clearly seen that TA has a broad absorption peak within 200–350 nm, while the fluorescence emission characteristic peak of ZnO QDs of Eu/ZIF-67@ZnO QDs is at 505 nm, and its absorption spectrum does not match with the luminescence spectrum of Eu/ZIF-67@ZnO QDs. According to the above results, we speculate that the fluorescence quenching of ZnO QDs is not caused by TA absorption, which excluding the fluorescence quenching caused by the fluorescence resonance energy transfer. In addition, the position of the UV absorption peak almost did not change before and after adding TA (Fig. 9(a)). As illustrated in Fig. 9(b), the UV absorption peak of Eu/ZIF-67@ZnO QDs occurs a blue-shift trend with the increase of the concentration of TA. So, it can be inferred that the formation of zincate complexes between TA and quantum dots due to the charge transfer. And it can be attributed to the dynamic collision between quantum dots and TA, resulting in electron transfer between quantum dots and aromatic groups of TA. As shown in Fig. 9(c), there is a good overlap

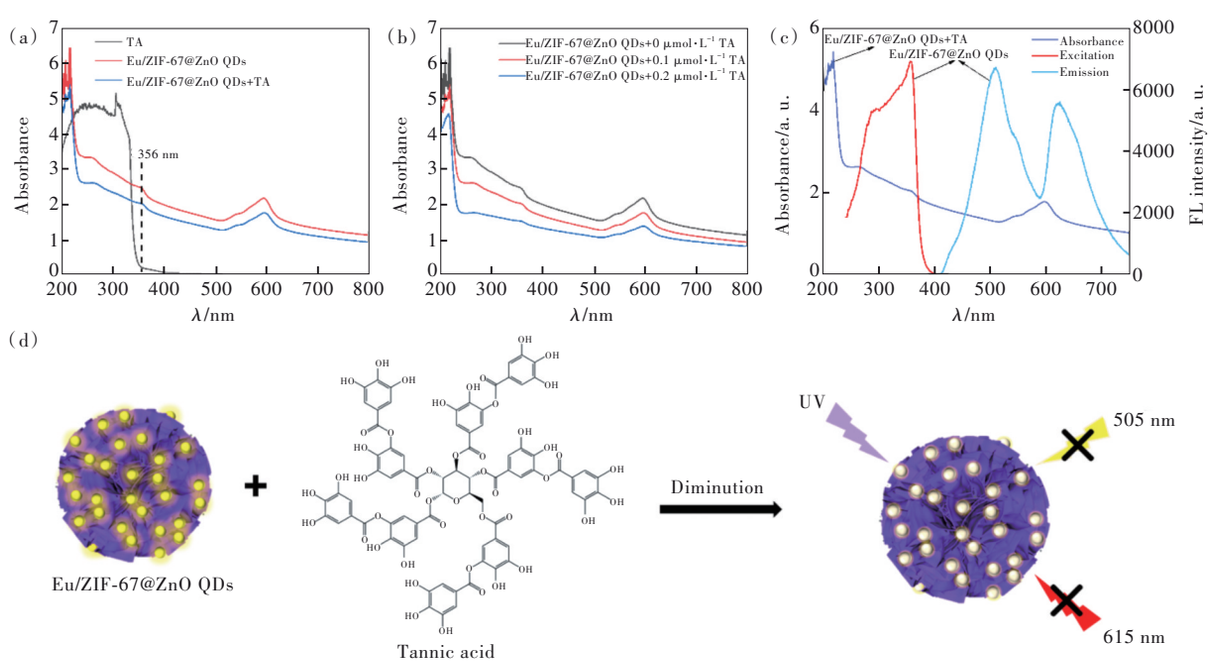

Fig.9　(a)UV-Vis spectroscopic of TA, Eu/ZIF-67@ZnO QDs, and Eu/ZIF-67@ZnO QDs +TA. (b)UV-Vis spectroscopic of Eu/ZIF-67@ZnO QDs with different concentrations of TA added. (c)The UV-Vis spectroscopic, excitation and emission spectrum of Eu/ZIF-67@ZnO QDs. (d)The mechanism of tannic acid detection by Eu/ZIF-67@ZnO QDs.

between the UV absorption spectra and the fluorescence excitation and emission spectra of Eu/ZIF-67@ZnO QDs, therefore, we speculate that the internal filtration effect is also one of the possible causes of the fluorescence burst. In summary, the fluorescence quenching of Eu/ZIF-67@ZnO QDs by TA may be generated based on the synergistic effects of both charge transfer and internal filtration effects[47].

4 Conclusion

In summary, a new pleated spherical zeolite-like imidazole ester skeleton material Eu/ZIF-67 was prepared by doping with lanthanide Eu, and amino-functionalized quantum dots ZnO QDs were successfully loaded on the surface to obtain a fluorescent hybrid material Eu/ZIF-67@ZnO QDs with double emission. It was found that this fluorescent hybrid material could achieve fluorescence detection of TA with good selective specificity and detection sensitivity, and the detection limit was as low as 0.029 9 μmol/L, and the fluorescence response could occur rapidly within 1 min. It provides a new idea for the economical and efficient measurement of TA concentration levels.

Response Letter is available for this paper at: http://cjl.lightpublishing.cn/thesisDetails#10.37188/CJL.20230048.

References:

[1] FIGUEROA-ESPINOZA M C, ZAFIMAHOVA A, ALVARADO P G M, *et al*. Grape seed and apple tannins: emulsifying and antioxidant properties [J]. *Food Chem.*, 2015, 178: 38-44.

[2] RICCI A, LAGEL M C, PARPINELLO G P, *et al*. Spectroscopy analysis of phenolic and sugar patterns in a food grade chestnut tannin [J]. *Food Chem.*, 2016, 203: 425-429.

[3] LU R F, ZHANG X Q, CHENG X X, *et al*. Medical applications based on supramolecular self-assembled materials from tannic acid [J]. *Front. Chem.*, 2020, 8: 583484-1-25.

[4] BALDWIN A, BOOTH B W. Biomedical applications of tannic acid [J]. *J. Biomater. Appl.*, 2022, 36(8): 1503-1523.

[5] AGUILERA J R, VENEGAS V, OLIVA J M, *et al*. Targeted multifunctional tannic acid nanoparticles [J]. *RSC Adv.*, 2016, 6(9): 7279-7287.

[6] CHOI J, YADAV S, WANG J Q, *et al*. Effects of supplemental tannic acid on growth performance, gut health, microbiota, and fat accumulation and optimal dosages of tannic acid in broilers [J]. *Front. Physiol.*, 2022, 13: 912797-1-23.

[7] NAKAMURA T, YOSHIDA N, YASOSHIMA M, *et al*. Effect of tannic acid on skin barrier function [J]. *Exp. Dermatol.*, 2018, 27(8): 824-826.

[8] PINTO A F, NASCIMENTO J MDO, SILVA SOBRAL R VDA, *et al*. Tannic acid as a precipitating agent of human plasma proteins [J]. *Eur. J. Pharm. Sci.*, 2019, 138: 105018-1-10.

[9] SONG B, YANG L W, HAN L L, *et al*. Metal ion-chelated tannic acid coating for hemostatic dressing [J]. *Materials*, 2019, 12(11): 1803-1-10.

[10] PICARIELLO L, GAMBUTI A, PETRACCA F, *et al*. Enological tannins affect acetaldehyde evolution, colour stability and tannin reactivity during forced oxidation of red wine [J]. *Int. J. Food Sci. Technol.*, 2018, 53(1): 228-236.

[11] RINALDI A, MOIO L. Effect of enological tannin addition on astringency subqualities and phenolic content of red wines [J]. *J. Sens. Stud.*, 2018, 33(3): e12325-1-11.

[12] DE FRANCESCO G, BRAVI E, SANARICA E, *et al*. Effect of addition of different phenolic-rich extracts on beer flavour stability [J]. *Foods*, 2020, 9: 1638-1-14.

[13] XIE C G, CUI H. Detection of tannic acid at trace level in industrial wastewaters using a highly sensitive chemiluminescence method [J]. *Water Res.*, 2003, 37(1): 233-237.

[14] WAN H J, ZOU Q L, YAN R, *et al*. Electrochemistry and voltammetric determination of tannic acid on a single-wall carbon nanotube-coated glassy carbon electrode [J]. *Microchim. Acta*, 2007, 159(1): 109-115.

[15] DA SILVA F G S, DOS SANTOS G K C, NETO S Y, *et al*. Self-powered sensor for tannic acid exploiting visible LED light as excitation source [J]. *Electrochim. Acta*, 2018, 274: 67-73.

[16] ZYWICKI B, REEMTSMA T, JEKEL M. Analysis of commercial vegetable tanning agents by reversed-phase liquid chromatography-electrospray ionization-tandem mass spectrometry and its application to wastewater [J]. *J. Chromatogr.* A, 2002, 970(1-2): 191-200.

[17] VARANKA Z, ROJIK I, VARANKA I, *et al.* Biochemical and morphological changes in carp (*Cyprinus carpio* L.) liver following exposure to copper sulfate and tannic acid [J]. *Comp. Biochem. Phys.* C *Toxicol. Pharmacol.*, 2001, 128(3): 467-478.

[18] 董英鸽, 杨金龙, 丁艳丽, 等. 反相微乳液法制备尺寸可调的高荧光碳量子点 [J]. 发光学报, 2015, 36(2): 157-162.
DONG Y G, YANG J L, DING Y L, *et al.* Size-controllable synthesis of highly fluorescent carbon quantum dots in a reverse microemusion [J]. *Chin. J. Lumin.*, 2015, 36(2): 157-162. (in Chinese)

[19] RANI P, DALAL R, SRIVASTAVA S. Study of electronic and optical properties of quantum dots [J]. *Appl. Nanosci.*, 2022, 12(7): 2127-2138.

[20] AL-ALWANI A J, SHINKARENKO O A, CHUMAKOV A S, *et al.* Influence of capping ligands on the assembly of quantum dots and their properties [J]. *Mater. Sci. Technol.*, 2019, 35(9): 1053-1060.

[21] 尚金梁, 卫迎迎, 王军丽, 等. 三苯甲基改性油溶性碳量子点合成及其在发光器件中的应用 [J]. 发光学报, 2021, 42(8): 1257-1266.
SHANG J J, WEI Y Y, WANG J L, *et al.* Synthesis of triphenylmethyl modified oil-soluble carbon quantum dots and their applications in light-emitting devices [J]. *Chin. J. Lumin.*, 2021, 42(8): 1257-1266. (in Chinese)

[22] YIN N Q, LI P, XU X L, *et al.* A dual-functional ferroferric oxide/quantum dots theranostic nanoplatform for fluorescent labeling and photothermal therapy [J]. *Part. Part. Syst. Charact.*, 2021, 38(6): 2100043-1-7.

[23] ZHENG S H, ZHANG M, BAI H Y, *et al.* Preparation of AS1411 aptamer modified Mn-MoS_2 QDs for targeted MR imaging and fluorescence labelling of renal cell carcinoma [J]. *Int. J. Nanomed.*, 2019, 14: 9513-9524.

[24] 湛志华, 陈芜而, 莫大幸, 等. 单激发双发射近红外荧光碳量子点制备、荧光性能与细胞成像 [J]. 发光学报, 2021, 42(8): 1307-1313.
ZHAN Z H, CHEN C E, MO D X, *et al.* Preparation, Fluorescent properties and cell imaging of near infrared fluorescent carbon quantum dots with single excited double emission [J]. *Chin. J. Lumin.*, 2021, 42(8): 1307-1313. (in Chinese)

[25] PRADHAN S. Multi-bandgap colloidal quantum dot mixing for optoelectronic devices [J]. *New J. Chem.*, 2022, 46(27): 12892-12900.

[26] YE Y F. Photoluminescence property adjustment of ZnO quantum dots synthesized *via* sol-gel method [J]. *J. Mater. Sci. Mater. Electron.*, 2018, 29(6): 4967-4974.

[27] GENG S, LIN S M, LIU S G, *et al.* Indirect detection of alcoholic strength in spirits by fluorescence method using the polyethyleneimine capped ZnO QDs [J]. *Sens. Actuators* B *Chem.*, 2016, 236: 591-596.

[28] YAMANI Z H, AL-JABARI M H, KHAN S A, *et al.* Colloidal solution of luminescent ZnO quantum dots embedded silica as Nano-tracers for remote sensing applications [J]. *J. Mol. Liq.*, 2019, 274: 447-454.

[29] 施周, 贺英, 蔡计杰, 等. ZnO@GQDs核壳结构量子点的制备及性能研究 [J]. 发光学报, 2014, 35(2): 137-141.
SHI Z, HE Y, CAI J J, *et al.* Synthesis and characterization of ZnO@Graphene quantum dots with core-shell structure [J]. *Chin. J. Lumin.*, 2014, 35(2): 137-141. (in Chinese)

[30] PIRZADEH K, ESFANDIARI K, GHOREYSHI A A, *et al.* CO_2 and N_2 adsorption and separation using aminated UiO-66 and $Cu_3(BTC)_2$: A comparative study [J]. *Korean J. Chem. Eng.*, 2020, 37(3): 513-524.

[31] ZHANG Y, LIU S, ZHAO Z S, *et al.* Recent progress in lanthanide metal-organic frameworks and their derivatives in catalytic applications [J]. *Inorg. Chem. Front.*, 2021, 8(3): 590-619.

[32] ZHANG Y, XU X, YAN B. A multicolor-switchable fluorescent lanthanide MOFs triggered by anti-cancer drugs: multifunctional platform for anti-cancer drug sensing and information anticounterfeiting [J]. *J. Mater. Chem.* C, 2022, 10(9): 3576-3584.

[33] 何睿夫, 周非凡, 屈军乐, 等. 金属有机框架材料在有机钙钛矿太阳能电池中的应用进展 [J]. 发光学报, 2021, 42(11): 1722-1738.
HE R F, ZHOU F F, QU J L, *et al.* Research progress of metal-organic frameworks in organic perovskite solar cells [J]. *Chin. J. Lumin.*, 2021, 42(11): 1722-1738. (in Chinese)

[34] MOGHADDAM E, YOUZBASHI A A, KAZEMZADEH A, *et al*. Photoluminescence investigation of ZnO quantum dots surface modified with silane coupling agent as a capping agent [J]. *J. Lumin.*, 2015, 168: 158-162.

[35] ZHANG X L, LUO S S, WU X D, *et al*. Effect of alkali bases on the synthesis of ZnO quantum dots [J]. *Open Chem.*, 2021, 19(1): 377-384.

[36] HUANG W Y, LV X W, TAN J L, *et al*. Regulable preparation of the oxygen vacancy of ZnO QDs and their fluorescence performance [J]. *J. Mol. Struct.*, 2019, 1195: 653-658.

[37] WANG W, ZHANG H, ZHAO Y Z, *et al*. A novel MOF-drived self-decomposition strategy for CoO@N/C-Co/Ni-$NiCo_2O_4$ multi-heterostructure composite as high-performance electromagnetic wave absorbing materials [J]. *Chem. Eng. J.*, 2021, 426: 131667.

[38] CHENG J, GUO H, YANG X, *et al*. Phosphotungstic acid-modified zeolite imidazolate framework (ZIF-67) as an acid-base bifunctional heterogeneous catalyst for biodiesel production from microalgal lipids [J]. *Energy Convers. Manage.*, 2021, 232: 113872-1-11.

[39] JUNG J Y, HONG Y L, KIM J G, *et al*. New insight of tailor-made graphene oxide for the formation of atomic Co-N sites toward hydrogen evolution reaction [J]. *Appl. Surf. Sci.*, 2021, 563: 150254-1-8.

[40] WANG Y Q, FANG Z, MIN H, *et al*. Sensitive determination of ofloxacin by molecularly imprinted polymers containing ionic liquid functionalized carbon quantum dots and europium ion [J]. *ACS Appl. Nano Mater.*, 2022, 5(6): 8467-8474.

[41] LI Y, YANG Y Q, JIANG Y M, *et al*. Detection of tannic acid exploiting carbon dots enhanced hydrogen peroxide/potassium ferricyanide chemiluminescence [J]. *Microchem. J.*, 2020, 157: 105113-1-7.

[42] YANG P, ZHU Z Q, CHEN M Z, *et al*. Microwave-assisted synthesis of polyamine-functionalized carbon dots from xylan and their use for the detection of tannic acid [J]. *Spectrochim. Acta* A *Mol. Biomol. Spectrosc.*, 2019, 213: 301-308.

[43] FALAK S, HUH D S. Iron oxide nanoparticles embedded in porous films for tannic acid detection [J]. *React. Funct. Polym.*, 2023, 183: 105494.

[44] PIOVESAN J V, SANTANA E R, SPINELLI A. A carbon paste electrode improved with poly(ethylene glycol) for tannic acid surveillance in beer samples [J]. *Food Chem.*, 2020, 326: 127055-1-6.

[45] ZHU X Y, YU J Y, YAN Y C, *et al*. One-pot alkali cutting-assisted synthesis of fluorescence tunable amino-functionalized graphene quantum dots as a multifunctional nanosensor for sensing of pH and tannic acid [J]. *Talanta*, 2022, 236: 122874-1-7.

[46] DA SILVA F G S, FERREIRA A R, DOS SANTOS C C, *et al*. Dual-photoelectrode photoelectrochemical cell exploiting a photoanode based on cadmium sulfide and anatase TiO_2 photocatalysts for tannic acid detection [J]. *J. Solid State Electrochem.*, 2021, 25(8): 2213-2224.

[47] 刘丽, 胡润泽, 徐陈, 等. 镧系 Eu^{3+}配合物修饰的分子印迹聚合物荧光探针制备及其对血红蛋白的传感检测 [J]. 发光学报, 2022, 43(6): 944-951.
LIU L, HU R Z, XU C, *et al*. Preparation of molecularly imprinted polymer fluorescence probe modified by lanthanide Eu^{3+} complex and hemoglobin sensing detection [J]. *Chin. J. Lumin.*, 2022, 43(6): 944-951. (in Chinese)

方舟(1998-),女,江苏淮安人,硕士研究生,2020年于大连大学获得学士学位,主要从事稀土荧光杂化材料的研究。
E-mail: ark2202@163.com

张栋梁(1986-),男,内蒙古包头人,博士,讲师,硕士生导师,2019年于北京化工大学获得博士学位,主要从事稀土光催化材料、稀土功能材料的研究。
E-mail: zdl20003@usst.edu.cn

李颖(1981-),女,内蒙古乌兰浩特人,博士,副教授,硕士生导师,2009年于同济大学获得博士学位,主要从事稀土/高分子荧光杂化材料及其生物化学传感应用的研究。
E-mail: liying@usst.edu.cn